Available online at www.sciencedirect.com
ScienceDirect
Materials Research Bulletin 43 (2008) 1519–1527
Materials Research Bulletin
www.elsevier.com/locate/matresbu

Preparation and characterization of $LiNiVO_4$ powder and non-stoichiometric $LiNi_xV_yO_z$ films

M.V. Reddy *, C. Wannek, B. Pecquenard, P. Vinatier, A. Levasseur

ICMCB/ENSCPB (CNRS UPR 9048), Université Bordeaux 1, 87 Avenue du Dr. Schweitzer 33608 Pessac Cedex, France

Received 3 January 2007; accepted 4 June 2007
Available online 12 June 2007

Abstract

Inverse spinel type structured oxide, $LiNiVO_4$, was synthesized by using solid-state method and the crystalline powder was characterized by Rietveld refinement and X-ray photoelectron spectroscopy. Non-stoichiometric lithium nickel vanadate thin films were prepared by physical vapour deposition technique. The amorphous films were characterized by Rutherford back-scattering spectroscopy (RBS), nuclear reaction analysis (NRA), Auger electron spectroscopy (AES), X-ray diffraction (XRD), scanning electron microscopy (SEM) and high-resolution transmission electron microscopy (HRTEM) analytical methods. Films crystal growth at various temperatures was also studied by XRD and SEM. The HRTEM analysis of sputtered film shows nanocrystalline domains of NiO and $LiNiVO_4$ phases with characteristic lattice parameters of the host compound and the results correlate well with the XRD data. Electrochemical properties of the films were discussed.

Keywords: A. Thin films; B. Sputtering; C. Electron diffraction; C. X-ray diffraction; D. Electrochemical properties

1. Introduction

Recently, metal oxide $LiNiVO_4$ (bulk and thin film) has been studied extensively in literature as an electrode material [1–10] for Li-ion batteries. Various methods of preparation and characterization are employed on optimizing morphology, structure and electrochemical performance of this material because it can be used as high-potential cathode material [1] and also high-capacity anode material [5]. Thin film solid-state batteries are of potential applications for the use in smart cards, implantable medical devices, CMOS, etc. because of their small ideal dimensions and high efficiency. In addition to energy storage, thin film materials are used as electrocatalysts, electrochromics, lubricants and so on.

Chemical, physical, microstructure, electronic and electrical properties of various non-stoichiometric transition metal oxides, electrode materials preparation and characterization have been studied in literature [10–14]. Recently, $LiNiVO_4$ films were prepared by radio frequency magnetron (rf) magnetron sputtering [7–9]. The composition, structure and morphology of films vary with the physical sputtering deposition parameters like power, total pressure and oxygen partial pressure and distance between target substrate and substrate temperature (in situ or ex situ).

* Corresponding author. Present address: Department of Physics, National University of Singapore, S12,03, Science Drive 3, Singapore 117542, Singapore. Tel.: +65 65162605; fax: +65 67776126.
E-mail address: phymvvr@nus.edu.sg (M.V. Reddy).

0025-5408/$ – see front matter
doi:10.1016/j.materresbull.2007.06.023

Fundamental and applied studies on non-stoichiometric thin film compositions in the amorphous or nanocrystalline/polycrystalline state showed interesting structural phases and morphology and physical properties [10–14]. Presently, we report Rietveld refinement of $LiNiVO_4$ powder and preparation and characterization of non-stoichiometric films by varying oxygen partial pressure during sputtering.

2. Experimental

2.1. Preparation of powder and target

The $LiNiVO_4$ crystalline powder was prepared by solid-state method. A stoichiometric mixture of high-purity (Aldrich) Li_2CO_3, NiO (prepared from decomposition of $Ni(NO_3)_2 6H_2O$) and V_2O_5 is heated at 550 °C for 2 h to eliminate carbonates, finally at 730 °C in air for 12 h at a heating rate of 3 °C/min. Final single phase product was used in fabrication of target. The target with a 5 mm diameter and 3 mm thickness was used for rf sputtering and target was prepared by using ~20 g of $LiNiVO_4$ powder and 5% stearin binder mixed well and finally cold pressed at ~260 MPa pressure. In order to remove binder and improve the robustness, the target was sintered at 600 °C for 8 h in a box furnace, in air.

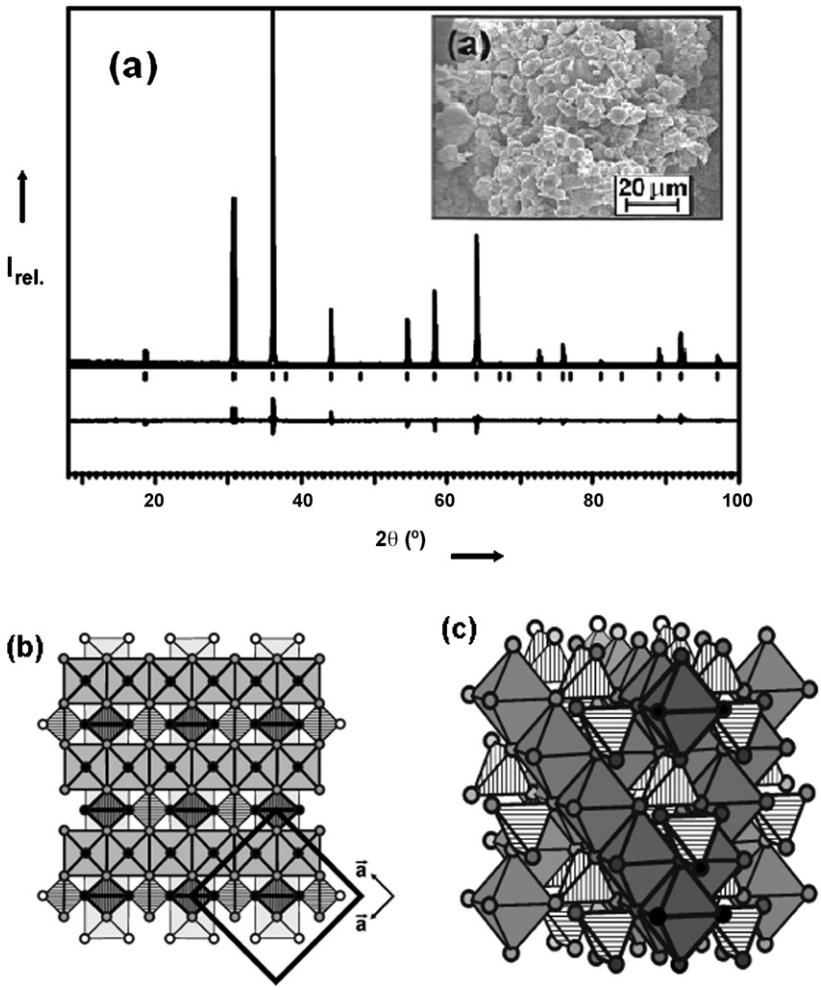

Fig. 1. (a) Rietveld-refined XRD pattern (continuous lines, top) of $LiNiVO_4$ powder, vertical bars represent positions of allowed (*h k l*) lines and difference pattern is also shown. (b, c) Crystallographic representation of $LiNiVO_4$ structure. Li, Ni ions are in octahedral site and V ions in tetrahedral site.

2.2. Thin films preparation and characterization

The radio frequency (rf) sputtering technique (physical vapour deposition technique) was used to fabricate lithium nickel vanadate films. The sputtering unit was placed in a dry-Argon glove box, to avoid contamination. The pure Argon (99.99%) was used as carrier gas, before sputtering of films; vacuum of $\sim 4 \times 10^{-5}$ Pa was applied into sputtering chamber for overnight. The sputtering conditions are: power, 30 W; oxygen partial pressure (P_{O_2}), 0 and 100 (10%) mPa gas; distance between target and substrate, 8 cm; total working pressure of Ar, 1 Pa; substrates are not heated during sputtering. Presputtering was carried out under identical conditions for 2 h duration to remove contaminated top target surface. For clarity thin films prepared at P_{O_2}: 0 mPa refer to compd. I and P_{O_2}: 100 (10%) mPa refer to compd. II. Thin films were deposited on various substrates depending on characterization method. Carbon (RBS/NRA) and stainless steel substrates (for electrochemical studies) were polished to get mirror finish by using silicon carbide paper. Finally, substrates were cleaned in distilled water and acetone by using ultrasonic bath, dried in an oven and transferred into a glove box. Silicon (1 1 1) and aluminium foil were used for SEM studies. High-resolution TEM measurements were carried out with the thin films (thickness ~200 Å) deposited directly on copper grid during sputtering. Here, we show TEM studies of only amorphous films prepared at $P_{O_2} = 0$ mPa and annealed films were not studied due to oxidation of Cu grids above 300 °C and samples are very fragile. In case of the annealed films, XRD studies give useful information about the structure of the films. The crystalline films are obtained by sintering the amorphous non-stoichiometric films deposited on Si substrates at various temperatures from 200 to 900 °C, for 2 h duration in a tubular furnace.

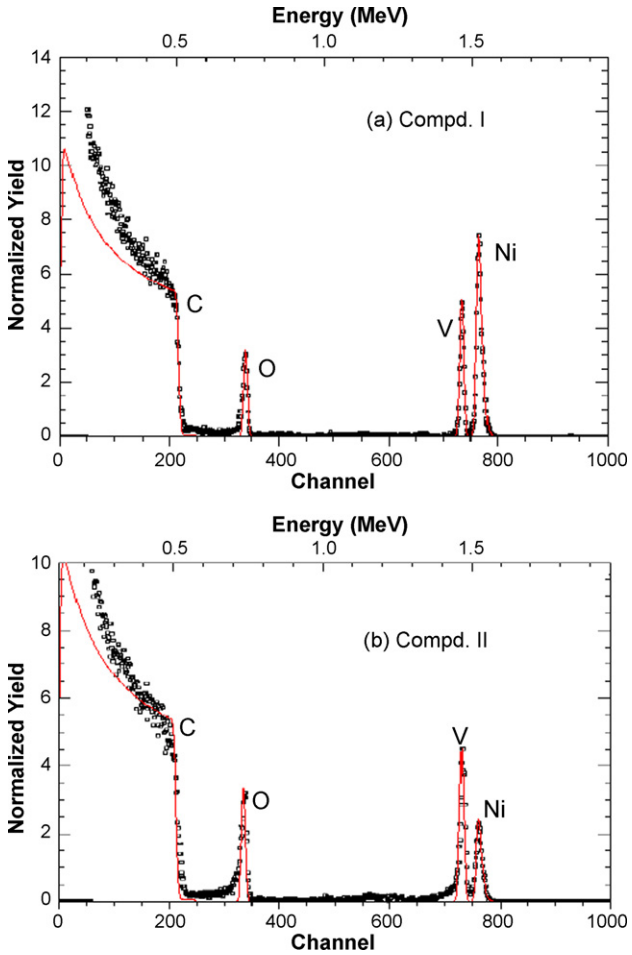

Fig. 2. RBS spectrum of $LiNi_xV_yO_z$ films of: (a) compd. I and (b) compd. II. *Symbols*: Open squares represent experimental RBS data and continuous lines represent simulated data by RUMP. Elements and substrate peaks are shown in figures.

The compositions of thin films were studied by Rutherford back-scattering technique (RBS), by using 2 MeV, $^4He^+$ ion beam. The experimental RBS spectrum was simulated by the use of Rutherford Universal Manipulation Program (RUMP) software. The lithium content was analysed by nuclear reaction analysis (NRA) ($^7Li(p\alpha)^4He$). The RBS and NRA measurements were performed at Nuclear Research Centre (CENBG), University of Bordeaux. The Auger electron spectroscopy (AES) (VG Micro lab 310F) was used to check depth profile of the films and also to give homogeneity. The structures of powder and thin films were studied by using X-ray diffractometer (XRD, Philips PW1730) with Cu Kα radiation. Rietveld refinement of powder was performed by using Fullprof software. X-ray photoelectron spectroscopy (XPS) analysis of the powder was performed by Surface Science Instruments spectrometer (model 301). Scanning electron microscopy (SEM) (JEOL JSM-5200 microscope) was used to study the surface morphology of the films. High-resolution electron microscopy (HRTEM) images were taken by using JEOL 3010 microscope. The electrochemical discharge–charge cycling was carried by using a galvanostic mode, 1 M $LiPF_6$ was used as electrolyte and cells were cycled in the range of 0.02–3.0 V, Li metal was used as counter and reference electrode.

3. Results and discussion

3.1. Characterization of $LiNiVO_4$ powder

The obtained $LiNiVO_4$ powder was in yellow colour. The Rietveld refinement X-ray diffraction pattern of the powder is shown in Fig. 1. The experimental spectra were refined with the space group $Fd\bar{3}m$ (2 2 7). The crystal parameters of the $LiNiVO_4$ powder are as follows: Li at the 16d site (5/8, 5/8, 5/8), occupancy 0.5, Beq ($Å^2$), 1.97(3);

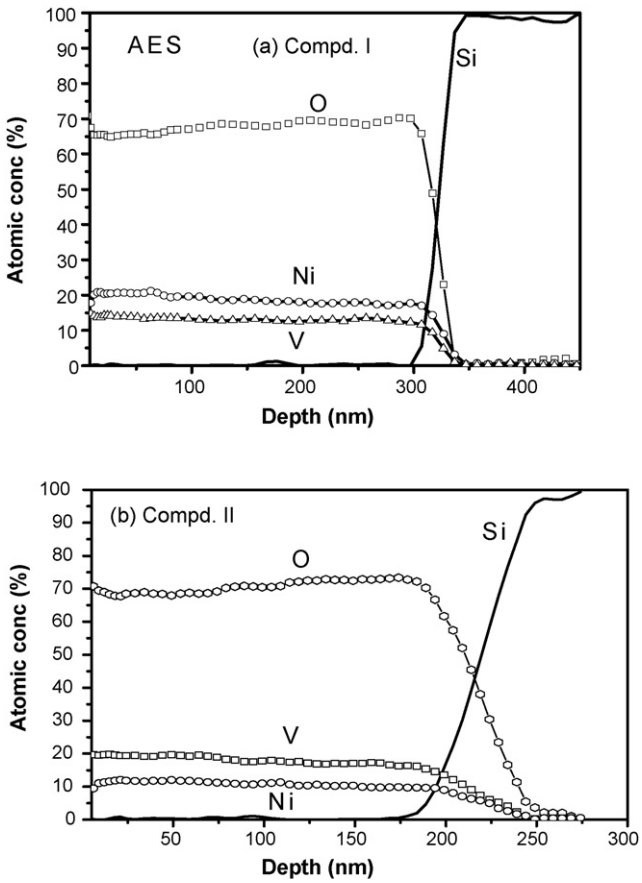

Fig. 3. AES atomic concentration vs. depth profile of: (a) compd. I and (b) compd. II.

Ni at the 16d site (5/8, 5/8, 5/8), occupancy 0.5, Beq (Å^2), 2.02(5); V at the 8a site (0,0,0), occupancy 1.0, Beq (Å^2), 1.78(3); O at the 32e site (0.3700(2), x, x), occupancy 0.5, Beq (Å^2), 2.24(6). The obtained lattice parameter value of $LiNiVO_4$ powder was $a = 8.21844(5)$ Å, $wR_p = 0.1118$, $R_B = 0.0340$, where $wR_p = [\sum w_i(y_{io} - y_{ic})2/\sum w_j y_{io}{}^2]^{1/2}$ and $R_B = \sum|I_{Ko} - I_{Kc}|/\sum I_{Ko}$, where y_{io} and y_{ic} represent the number of counts observed and calculated, w_i the statistical factor, I_o and I_c are the observed and calculated intensity. The crystallographic representation of $LiNiVO_4$ structure is shown in Fig. 1b and c. The lattice parameter of the compound agrees well with Bernier et al. ($a = 8.215$ Å) [15] and Liu et al. ($a = 8.223$ Å) [4]. The X-ray photoelectron spectroscopy studies of $LiNiVO_4$ showed binding energy of Ni $2P_{3/2}$, 855.1 eV; V $2P_{3/2}$, 516 eV; Li 1s, 54.6 eV; O 2P, 529.6 eV. The SEM photograph shows (Fig. 1a) agglomerated particles with sizes ranging from 6 to 10 μm.

3.2. Chemical composition of thin films

Rutherford back-scattering spectrometry has been widely used for surface analysis by nuclear physicists [16]. It provides a rapid and simple method of examining films purity, composition and thickness. The experimental RBS spectra are shown in Fig. 2a and b. For convenience, compd. I (P_{O_2}: 0 mPa) and compd. II (P_{O_2}: 100 mPa) refer to former and later composition, respectively. The RBS spectra clearly show a peak corresponding to energy channel

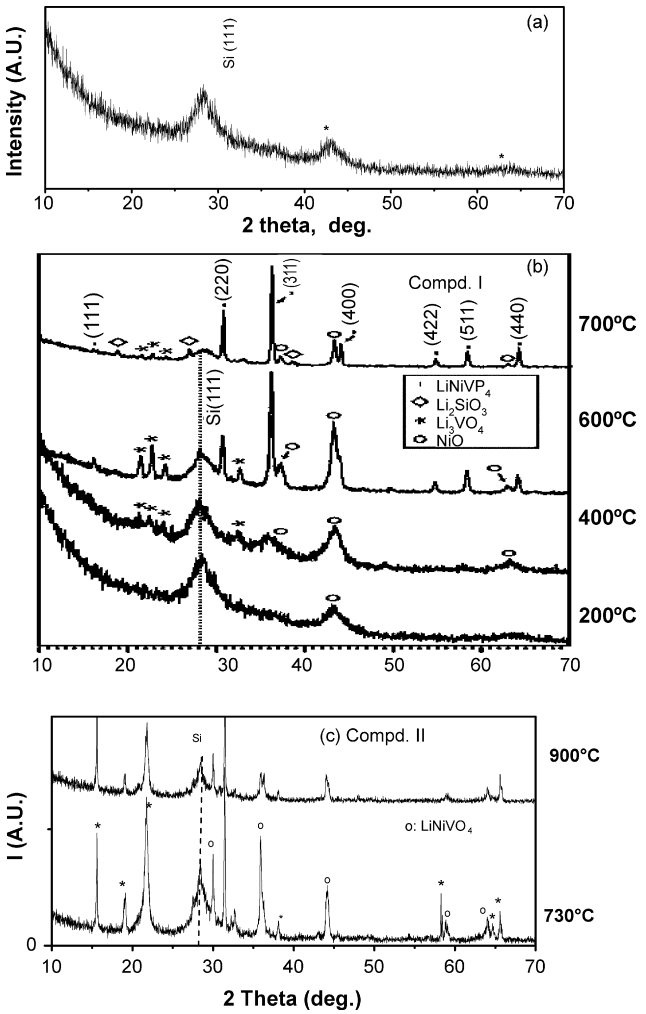

Fig. 4. X-ray diffraction pattern of: (a) as-deposited film and (b) annealed films of compd. I and (c) compd. II annealed film with Cu Kα radiation. Film thickness $t > 1$ μm; silicon (1 1 1) substrate; 2 h annealing time and temperature are indicated in figures.

numbers of Ni, V, O and C elements, where C peak is due to the substrate and absence of other surface impurities in the spectra. The simulated spectra (continuous line) by RUMP software of the compds. I and II are shown in Fig. 2a and b. The chemical composition of compds. I and II were $LiNi_1V_{0.75\ (\pm0.03)}O_{3.4(\pm0.1)}$ and $LiNi_1V_{1.6\ (\pm0.03)}O_{5.8(\pm0.1)}$ respectively and these values are in good agreement with peaks area (Ni, V, O) (Fig. 2). The lithium content was not determined using RBS due to its low surface scattering and matrix scattering height, these values of $LiNiVO_4$ film were reported elsewhere [6]. The NRA analysis shows that lithium contents of compds. I and II were $Li_{1\ (\pm0.1)}$ and $Li_{1.3\ (\pm0.1)}$, respectively. AES plots of atomic concentration versus depth profiles of compds. I and II are shown in Fig. 3. The sputtered films are homogeneous with thickness, this shows uniform deposition of elements (Ni, V, O) during sputtering time irrespective of deposition conditions, except for compositional (atomic concentration) variation. The

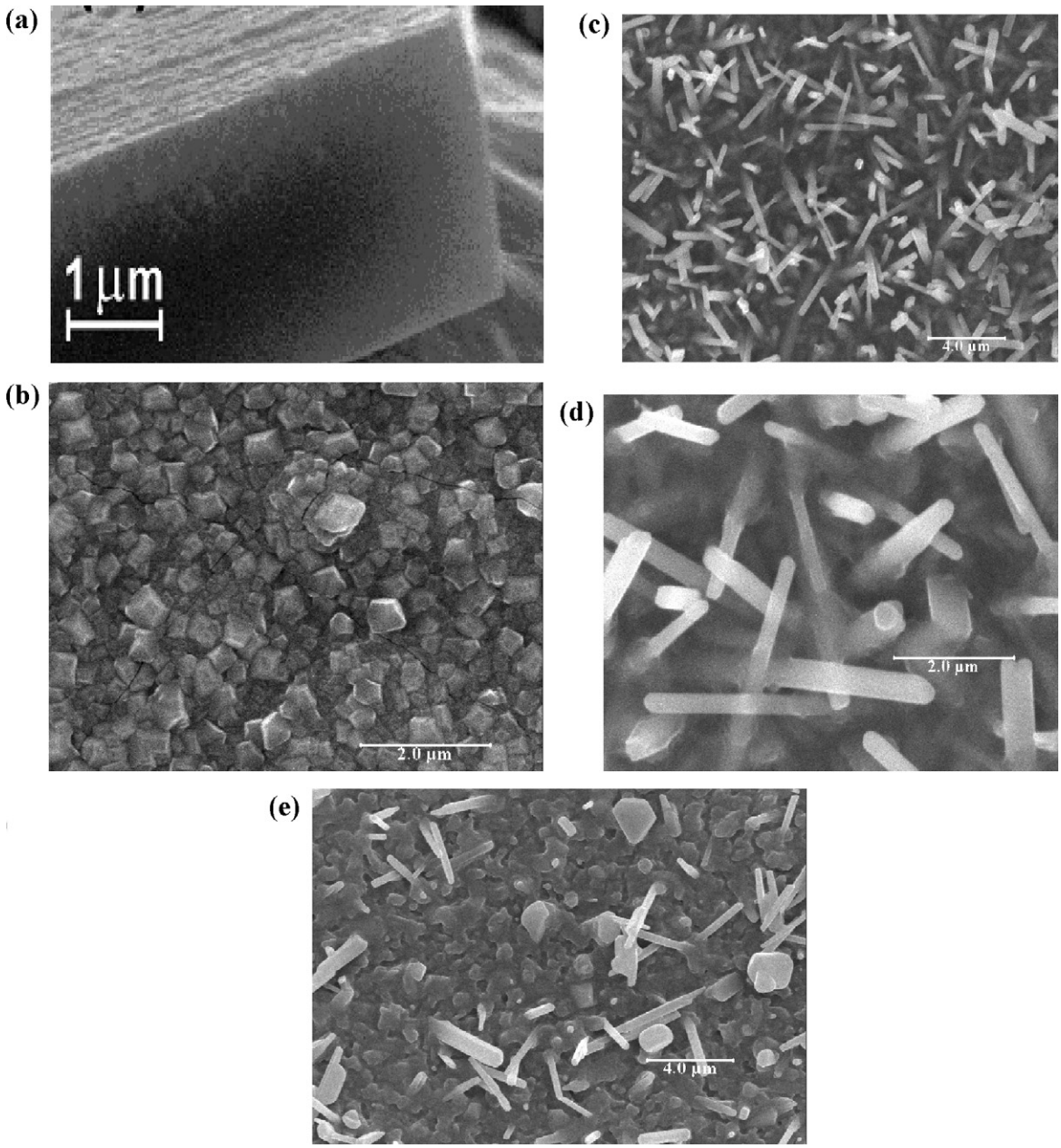

Fig. 5. SEM photographs of films of: (a) compd. I, amorphous, bar scale, 1 μm; (b) compd. I, annealed films at 730 °C, bar scale 2.0 μm; (c) compd. II, annealed at 730 °C, bar scale 4.0 μm; (d) same as (c) in expanded scale; (e) compd. II, annealed at 900 °C, bar scale, 4.0 μm. Annealing time, 2 h.

lithium depth profile of the non-stoichiometric films with thickness by NRA analysis is not studied, we assume from our previous studies on Li concentration analysis of stoichiometric films that Li-concentrations are in good homogeneity with the thickness of the film, more details on analysis are discussed previously [6].

3.3. Crystal structure of films

The colour of deposited films varies depending on film thickness, it varies from green, brown, yellow and black (>1 μm). The XRD patterns of the as-deposited sputtered film of compd. I are shown in Fig. 4a. The broad peaks in the XRD pattern are characteristic of amorphous nature of film; broad peaks correspond to NiO (2 0 0) and also $LiNiVO_4$ films (4 0 0). In the amorphous films, it is difficult to differentiate exact phases (*h k l*) lines [NiO (2 0 0) or $LiNiVO_4$ (4 0 0)]. To understand the nature of these (*h k l*) lines and the structure and crystal growth of the films, we studied the effect of annealing temperature on the growth of the $LiNi_xV_yO_z$ films (compds. I and II) studied by using XRD. The XRD patterns of the compd. I at various annealing temperatures (200–700 °C) are shown in Fig. 4b. Intensity of (2 2 0) *h k l* line is much stronger than (1 1 1) line due to the presence of transition metal atom (V) in tetrahedral site, whereas normal spinel like $LiMn_2O_4$ (1 1 1) line is strongest and (2 2 0) is the weakest line. XRD diagrams of the annealed film of the compd. I showed a major phase of $LiNiVO_4$ in addition to NiO, Li_3VO_4 are present as impurity phases where as compd. II shows a mixture of LiV_2O_5 or Li_3VO_4 and $LiNiVO_4$ phases are shown in Fig. 4c. The XRD patterns of annealed films (compds. I, II) correlate well with the chemical compositions obtained from RBS analysis.

3.4. Morphology, nanostructure and electrochemical studies

The SEM images of the compds. I and II are shown in Fig. 5. As-deposited films are dense in morphology. The compds. I and II show as-expected variation of particle size/morphology with annealing temperature. The compd. I shows submicron-sized particles (Fig. 5b) and interestingly the compd. II shows a rod-like morphology, these films on

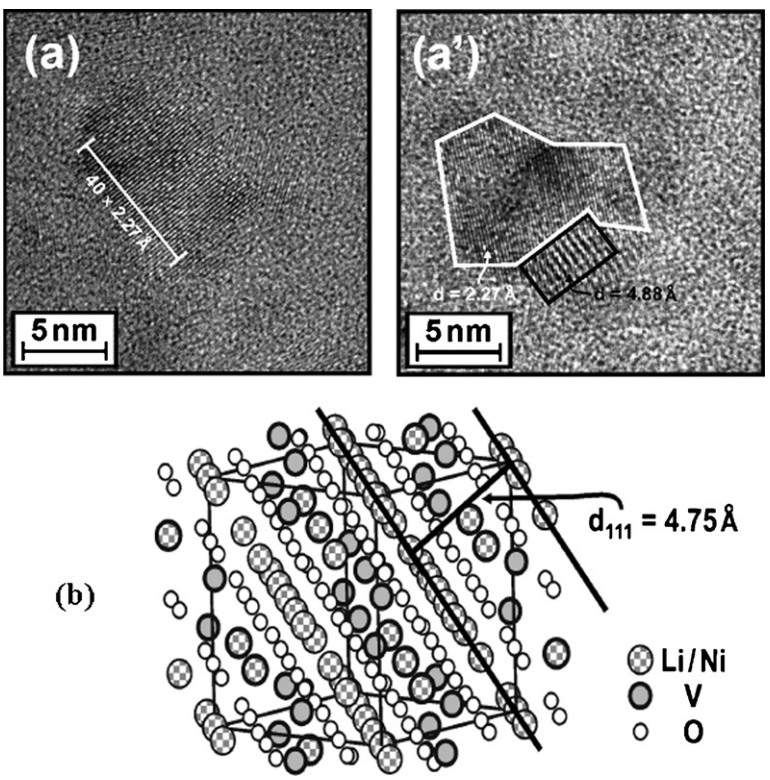

Fig. 6. (a and a′) High-resolution TEM images of amorphous film of compd. I ∼200 Å thick sputtered on copper grid; (b) Schematic view of ($d_{1\,1\,1}$) line in $LiNiVO_4$ structure.

further heating at high temperature, variation of surface morphology, particle size are clearly seen in Fig. 5e. In addition, the particle size varies with thickness of the films, smaller thickness ($\leq$0.3 μm) particle is lesser compared to thick films ($\geq$1 μm). The HRTEM images of compd. I are shown in Fig. 6a and a′. The photographs clearly show as-deposited films are in amorphous nature and in addition to two types of nanocrystallite domains are clearly seen in Fig. 6a′. The nanodomain corresponds to lattice spacing of NiO (d) = 2.27 Å and $LiNiVO_4$ (d) = 4.8 ($\pm$0.1) Å compounds. These d-values of compd. I compare well with the $d_{(1\ 1\ 1)}$ line of the host $LiNiVO_4$ (d = 4.75 Å) and schematic diagram ($d_{1\ 1\ 1}$) lines in the host compound are displayed in Fig. 6b. Our studies showed that crystallite nanodomains vary depending on deposition rate and reactive gas [7,11,12]. In general morphology, crystallite size of the sputtered films depends on mobility (i.e. low mobility or medium to high mobility) of the atoms [17].

The electrochemical charge–discharge cycles of the compds. I and II are shown in Fig. 7a and b cycled in the potential range of 0.02–3.0V and at a current density of 10 μA cm^2. The first discharge cycle plots clearly show voltage plateaus at ~1.70 V, ~0.75 V and cycling plots are characteristic nature of amorphous films. During first discharge

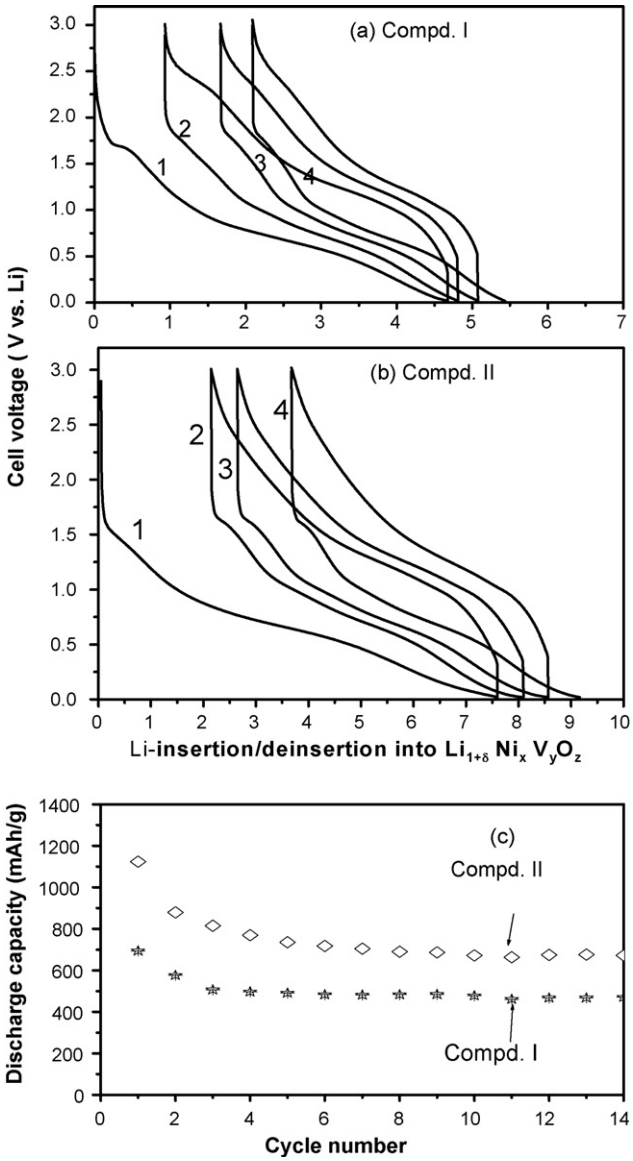

Fig. 7. (a–c) Galvanostatic discharge–charge cycling plots of compds. I and II. Voltage range, 3.0–0.02 V; current density, 10 μA/cm^2; geometrical area of the electrode, 1.32 cm^2. Number in figures represents discharge–charge cycle number.

cycle of the compds. I and II, 4.7–7.5 moles of lithium are inserted into the host compound which corresponds to a capacity of 690 and 1130 (±30) mAh/g. The capacity versus cycle number plots of the compds. I and II is shown in Fig. 7c and compds. I and II deliver a reversible (1st charge) capacity of 550 and 820 mAh/g. Indeed stoichiometric $LiNiVO_4$ films deliver a superior capacity depending on structure and morphology and annealing temperature [7,9]. The reasons for the variation in electrochemical properties are due to compositional variation, morphology and structural defects in the films.

4. Conclusions

In this paper, we prepared $LiNiVO_4$ powder and characterized it by Rietveld refinement and XPS. $LiNi_xV_yO_z$ thin films were prepared by using rf magnetron sputtering in absence of oxygen and high partial pressure of oxygen (10%) during deposition. The compositions of films were systematically studied by RBS, NRA. Sputtered films are homogeneous with thickness conformed by AES. SEM analysis showed that films morphology varies with sputtering conditions, annealing temperature and composition of the films. XRD analysis showed as-deposited films are amorphous and nano/polycrystalline/crystalline films are formed by annealing treatment. HRTEM analysis of the as-deposited film showed a nanocrystalline nature with a characteristic lattice spacing of the host compound. Electrochemical properties of films during 1st discharge capacity ranges from 690 to 1130 (±30) mAh/g.

Acknowledgements

Thanks are due to N. Martz, Department of Material Science, Technical University of Darmstadt, Germany, for help with TEM; P. Moretto, CENBG, University of Bordeaux, for his help with RBS and NRA measurements; M. Lahaye, ICMCB-CNRS, for help with AES; D. Gonbeau, LCTPCM, Pau, France, for help with XPS analysis.

References

[1] G.T.K. Fey, P. Muralidharan, C.Z. Lu, Y.-D. Cho, Solid State Ionics 177 (2006) 877.
[2] A. Subramania, N. Angayarkanni, S.N. Karthick, T. Vasudevan, Mater. Lett. 60 (2006) 3023.
[3] Z. Zhongqiang, M. Junfeng, X. Lijin, T. Hua, Z. Jun, H. Yingmo, H. Xiang, W. Pingwei, D. Jinhui, Z. Zhibin, W. Hongfen, C. Haiyan, J. Am. Chem. Soc. 88 (2005) 2622.
[4] R.S. Liu, Y.C. Cheng, R. Gundakaran, L.Y. Jang, Mater. Res. Bull. 36 (2001) 1479.
[5] F. Orsini, E. Baudrin, S. Denis, L. Dupont, M. Touboul, D. Guyomard, Y. Piffard, J.-M. Tarascon, Solid State Ionics 107 (1998) 123.
[6] C. Rossignol, G. Ouvrard, E. Baudrin, J. Electrochem. Soc. 148 (2001) A869.
[7] M.V. Reddy, B. Pecquenard, P. Vinatier, A. Levasseur, J. Phys. Chem. B 110 (2006) 4301.
[8] M.V. Reddy, B. Pecquenard, P. Vinatier, C. Wannek, A. Levasseur, P. Moretto, Nucl. Instrum. Methods Phys. Res. B 246 (2006) 397.
[9] M.V. Reddy, B. Pecquenard, P. Vinatier, A. Levasseur, J. Power Sources 163 (2007) 1040.
[10] E. Schmidt, F. Weill, G. Meunier, A. Levasseur, Thin Solid Films 245 (1994) 34.
[11] I. Martin-Litas, P. Vinatier, A. Levasseur, J.C. Dupin, D. Gonbeau, F. Weill, Thin Solid Films 416 (2002) 1.
[12] K.J. Rao, H. Benqlilou-Moudden, G. Couturier, P. Vinatier, A. Levasseur, Mater. Res. Bull. 37 (2002) 1353.
[13] I. Martin-Litas, P. Vinatier, A. Levasseur, J.C. Dupin, D. Gonbeau, Bull. Mater. Sci. 26 (2003) 673.
[14] K.J. Rao, B. Pecquenard, A. Gies, A. Levasseur, J. Etourneau, Bull. Mater. Sci. 29 (2006) 535.
[15] J.C. Bernier, P. Poix, A. Michel, Bull. Soc. Chim. Fr. (1963) 445.
[16] K.-P. Lieb, Contemp. Phys. 40 (1999) 385.
[17] R.J. Messier, Vac. Sci. Technol. A 4 (1986) 490.